

---

# Residual Pathway Priors for Soft Equivariance Constraints

---

Marc Finzi\*  
New York University

Gregory Benton\*  
New York University

Andrew Gordon Wilson  
New York University

## Abstract

There is often a trade-off between building deep learning systems that are expressive enough to capture the nuances of the reality, and having the right inductive biases for efficient learning. We introduce Residual Pathway Priors (RPPs) as a method for converting hard architectural constraints into soft priors, guiding models towards structured solutions, while retaining the ability to capture additional complexity. Using RPPs, we construct neural network priors with inductive biases for equivariances, but without limiting flexibility. We show that RPPs are resilient to approximate or misspecified symmetries, and are as effective as fully constrained models even when symmetries are exact. We showcase the broad applicability of RPPs with dynamical systems, tabular data, and reinforcement learning. In Mujoco locomotion tasks, where contact forces and directional rewards violate strict equivariance assumptions, the RPP outperforms baseline model-free RL agents, and also improves the learned transition models for model-based RL.

## 1 Introduction

Central to the expanding application of deep learning to structured data like images, text, audio, sets, graphs, point clouds, and dynamical systems, has been a search for finding the appropriate set of inductive biases to match the model to the data. These inductive biases, such as recurrence [46], local connectivity [32], equivariance [10], or differential equations [8], reduce the set of explored hypotheses and improve generalization. Equivariance in particular has had a large impact as it allows ruling out a large class of meaningless shortcut features in many distinct domains, such as the ordering of the nodes in graphs and sets or the coordinate system chosen for an image.

A disadvantage of hard coding these restrictions is that this prior knowledge may not match reality. A scene may have long range non-local interactions, rotation equivariance may be violated by a preferred camera angle, or a dynamical system may occasionally have discontinuous transitions. In particular, symmetries are delicate. A small perturbation like adding wind breaks the rotational symmetry of a pendulum, and bumpy or tilted terrain could break the translation symmetry for locomotion. In these cases we would like to incorporate our prior knowledge in a way that admits our own ignorance, and allows for the possibility that the world is more complex than we imagined. We aim to develop an approach that is more general, and can be applied when symmetries are exact, approximate, or non-existent.

The Bayesian framework provides a mechanism for expressing such knowledge through priors. In much of the past work on Bayesian neural networks, the relationship between the prior distribution and the functions preferred by the prior is not transparent. While it is easy to specify different variances for different channels, or to use heavy tailed distributions, it is hard know how high level properties meaningfully translate into these low level attributes. Ultimately priors should represent our prior *beliefs*, and the beliefs we have are about high level concepts like the locality, independence, and symmetries of the data.

---

\*Equal Contribution

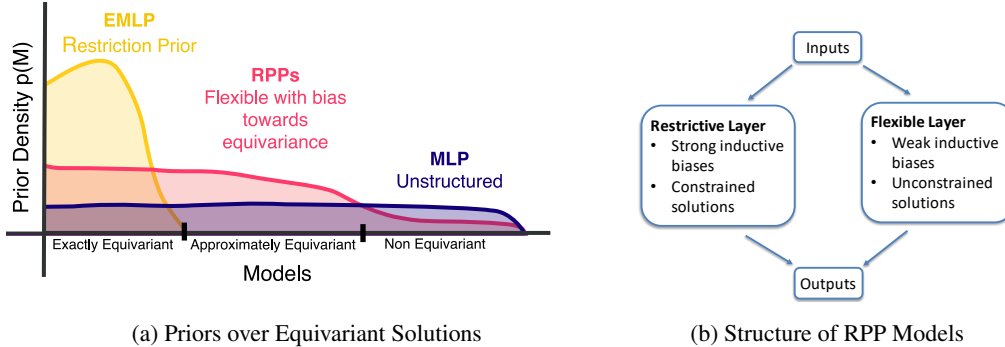


Figure 1: **Left:** RPPs encode an Occam’s razor approach to modeling. Highly flexible models like MLPs lack the inductive biases to assign high prior mass to relevant solutions for a given problem, while models with strict constraints are not flexible enough to support solutions with only approximate symmetry. For a given problem, we want to use the most constrained model that is consistent with our observations. **Right:** The structure of RPPs. Expanding the layers into a sum of the constrained and unconstrained solutions, while setting the prior to favor the constrained solution, leads to the more flexible layer explaining only the *residual* of what is already explained by the constrained layer.

To address the need for more interpretable priors we introduce *Residual Pathway Priors* (RPPs), a method for converting hard architectural constraints into soft priors. Practically, RPPs allow us to tackle problems in which perfect symmetry has been violated, but approximate symmetry is still present, as is the case for most real world physical systems. RPPs have a prior bias towards equivariant solutions, but are not constrained to them.

We use the schematic in Figure 1a as an approach to model construction [57, 37]. The flexibility of our model is described by what solutions have non-zero prior probability density. The *inductive biases* are described by the distribution of support over solutions. We wish to construct models with inductive biases that assign significant prior mass for solutions we believe to be a priori likely, but without ruling out other solutions we believe to be possible. For example, models constrained to exact symmetries could not fully represent many problems, such as the motion of a pendulum in the presence of wind. Flexible models with poor inductive biases, spread thinly across possible solutions, could express an approximate symmetry, but such solutions are unlikely to be found because of the low prior density. In this sense, we wish to embrace a notion of Occam’s razor such that “everything should be made as simple as possible, but no simpler”.

As we find with problems in which symmetries exist, highly flexible models with weak inductive biases like MLPs fail to concentrate prior mass around solutions that exhibit any symmetry. On the other hand when symmetries are only approximate, the strong restriction biases of constrained models like Equivariant Multi-Layer Perceptrons (EMLP) [17] fail to provide support for the observations. As a middle ground between these two extremes, RPPs combine the inductive biases of constrained models with the flexibility of MLPs to define a model class which excels when data show approximate symmetries, as shown in Figure 1b.

In the following sections we introduce our method and show results across a variety of domains. We list our contributions and the accompanying sections below:

1. We propose *Residual Pathway Priors* as a mechanism to imbue models with soft inductive biases, without constraining flexibility.
2. While our approach is general, we use RPPs to show how to turn hard architectural constraints into soft equivariance priors (Section 4).
3. We demonstrate that RPPs are robust to varying degrees of symmetry (Section 5). RPPs perform well under exact, approximate, or misspecified symmetries.
4. Using RPP on the approximate symmetries in the complex state spaces of the Mujoco locomotion tasks, we improve the performance of model free RL agents (Section 6).

We provide a PyTorch implementation of residual pathway priors at <https://github.com/mfinzi/residual-pathway-priors>.

## 2 Related Work

The challenge of equivariant models not being able to fully fit the data has been identified in a number of different contexts, and with different application specific adjustments to mitigate the problem. Liu et al. [35] observe that convolutional networks can be extremely poor at tasks that require identifying or outputting spatial locations in an image as a result of the translation symmetry. The authors solve the problem by concatenating a coordinate grid to the input of the convolution layer. Constructing translation and rotation equivariant GCNNs, Weiler and Cesa [56] find that in order to get the best performance on CIFAR-10 and STL-10 datasets which have a preferred camera orientation, they must break the symmetry, which they do by using equivariance to progressively smaller subgroups in the later layers. Bogatskiy et al. [6] go to great lengths to construct Lorentz group equivariant networks for tagging collisions in particle colliders only to break the symmetry by introducing dummy inputs that identify the collision axis. van der Wilk et al. [53] use the marginal likelihood to learn approximate invariances in Gaussian processes from data. In a related procedure, Benton et al. [5] learn the *extent* of symmetries in neural networks using the reparametrization trick and test time augmentation. While sharing some commonalities with RPP, this method is not aimed at achieving approximate equivariance and cannot bake equivariance into the model architecture.

A separate line of work has attempted to combine the extreme flexibility of the Vision Transformer (ViT) [13] with the better sample efficiency of convolutional networks, by incorporating convolutions at early layers [59] or making the self attention layer more like a convolution [12, 11]. Most similar to our work, ConViT [12] uses a gating mechanism for adding a soft locality bias to the self attention mechanism in Vision Transformers. ConViT and RPP share the same motivation, but while ConViT is designed specifically for biasing towards locality in the self attention layer, RPP is a general approach that we can apply broadly with other kinds of layers, symmetries, or architectural constraints.

Outside of equivariance, adding model outputs to a much more restrictive base model has been a fruitful idea employed in multiple contexts. The original ResNet [23, 24] drew on this motivation, with shortcut connections. Johannink et al. [27] and Silver et al. [48] proposed Residual Reinforcement Learning, whereby the RL problem is split into a user designed controller using engineering principles and a flexible neural network policy learned with RL. Similarly, in modeling dynamical systems, one approach is to incorporate a base parametric form informed by models from physics or biology, and only learn a neural network to fit the delta between the simple model and reality [28, 36].

There have been several works tackling symmetries and equivariance in RL, such as permutation equivariance for multi-agent RL [49, 26, 34], as well exploring reflection symmetry for continuous control tasks [1], and discrete symmetries in the more general framework of MDP homomorphisms [52]. However, in each of these applications the symmetries need to be exact, and the complexities of real data often require violating those symmetries. Although not constructed with this purpose, some methods which use regularizers to enforce equivariance [51] could be used for approximate symmetries. Interestingly, the value of approximate symmetries of MDPs has been explored in some theoretical work [45, 50], but without architectures that can make use of it. Additionally, data augmentation, while not able to bake in architectural equivariance, has been successfully applied to encouraging equivariance on image tasks [30] and recently even on tabular state vectors [33, 40].

## 3 Background

In order to develop our method, we first review the concept of group symmetries, how representations formalize the way these symmetries act on different objects.

**Group Symmetries** In the machine learning context, a symmetry group  $G$  can be understood as a set of invertible transformations under which an object is the same, such as reflections or rotations. These symmetries can act on many different kinds of objects. A rotation could act on a simple vector, a 2d array like an image, a complex collection of objects like the state space of a robot, or more abstractly on an entire classification problem or Markov Decision Process (MDP).

**Representations** The way that symmetries act on objects is described by a *representation*. Given an object in an  $n$ -dimensional vector space  $V$ , a group representation is a mapping  $\rho : G \rightarrow \mathbb{R}^{n \times n}$ , yielding a matrix which acts on  $V$ . Vectors  $v \in V$  are transformed  $v \mapsto \rho(g)v$ . In deep learning, each of the inputs and outputs to our models can be embedded in some vector space: an  $m \times m$  sized

rgb image exists in  $\mathbb{R}^{3m^2}$ , and a node valued function on a graph of  $m$  elements exists within  $\mathbb{R}^m$ . The representation  $\rho$  specifies how each of these objects transform under the symmetry group  $G$ .

These representations can be composed of multiple simpler subrepresentations, describing how each object within a collection transforms. For example given the representation  $\rho_1$  of rotations acting on a vector in  $\mathbb{R}^3$ , and a representation  $\rho_2$  of how rotations act on a  $3 \times 3$  matrix, the two objects concatenated together have a representation given by  $\rho_1(g) \oplus \rho_2(g) = \begin{bmatrix} \rho_1(g) & 0 \\ 0 & \rho_2(g) \end{bmatrix}$ , where the two matrices are concatenated along the diagonal. Practically this means we can represent intricate and multifaceted structures by breaking them down into their component parts and defining how each part transforms. For example, we may know that the velocity vector, an orientation quaternion, a joint angle, and a control torque all transform in different ways under a left-right reflection, and one can accommodate this information into the representation.

**Equivariance** Given some data  $X$  with representation  $\rho_{\text{in}}$ , and  $Y$  with representation  $\rho_{\text{out}}$ , we may wish to learn some mapping  $f : X \rightarrow Y$ . A model  $f$  is equivariant [10], if applying the symmetry transformation to the input is equivalent to applying it to the output

$$f(\rho_{\text{in}}(g)x) = \rho_{\text{out}}(g)f(x).$$

In other words, it is not the symmetry of  $X$  or  $Y$  that is relevant, but the symmetry of the function  $f$  mapping from  $X$  to  $Y$ . If the true relationship in the data has a symmetry, then constraining the hypothesis space to functions  $f$  that also have the symmetry makes learning easier and improves generalization [15]. Equivariant models have been developed for a wide variety of symmetries and data types like images [10, 58, 61, 56], sets [60, 39], graphs [38], point clouds [3, 18, 47], dynamical systems [16], jets [6], and other objects [54, 17].

## 4 Residual Pathway Priors

In this section, we introduce Residual Pathway Priors (RPPs). The core implementation of the RPP is to expand each layer in model into a sum of both a restrictive layer that encodes the hard architectural constraints and a generic more flexible layer, but penalize the more flexible path via a lower prior probability. Through the difference in prior probability, explanations of the data using only the constrained solutions are prioritized by the model; however, if the data are more complex the residual between the target and the constrained layer will be explained using the flexible layer. We can apply this procedure to any restriction priors, such as linearity, locality, Markovian structure, and, of course, equivariance.

The Residual Pathway Prior draws inspiration from the residual connections in ResNets [23, 24], whereby training stability and generalization improves by providing multiple paths for gradients to flow through the network that have different properties. One way of interpreting a residual block and shortcut connection  $f(x) = x + h(x)$  in combination with l2 regularization, either explicitly from weight decay or implicitly from the training dynamics [43], is as a prior that places higher prior likelihood on the much simpler identity mapping than on the more flexible function  $h(x)$ . In this way,  $h(x)$  need only explain the the difference between what is explained in the previous layer (passed through by  $I$ ) and the target.

We can leverage a similar approach to convert the hard constraints of a restriction prior specified through a given network architecture into a soft prior that merely places higher prior density on such models. Supposing we have an equivariant layer  $A(x)$ , and a more flexible non-equivariant layer  $B(x)$  which contains  $A$  as a special case, we can allow the model to explain part of the data with  $A$ , and part with  $B$ , by forming the sum  $A(x) + B(x)$ . Given a prior on the size of  $A$  and  $B$ , such as  $p(A) \propto \exp(-\|A\|^2/2\sigma_a^2)$ , and  $p(B) \propto \exp(-\|B\|^2/2\sigma_b^2)$  with  $\sigma_a > \sigma_b$ , a MAP optimized model will favor explanations of the data using the more structured layer  $A$ , and only resort to using layer  $B$  to explain the *difference* between the target and what is already explained by the more structured model  $A$ . Adding these non-equivariant residual pathways to each layer of an equivariant model, we have a model that has the same expressivity of a network formed entirely of  $B$  layers, but with the inductive bias towards a model formed entirely with the equivariant  $A$  layers. We term this model a *Residual Pathway Prior*.

To make the approach concrete, we first consider constructing equivariance priors using the constraint solving approach known as Equivariant Multi-Layer Perceptrons (EMLP) from Finzi et al. [17].

**Equivariant MLPs** EMLPs provide a method for automatically constructing exactly equivariant layers for any given group and representation by solving a set of constraints. The way in which the vectors are equivariant is given by a formal specification of the types of the input and output through defining their representations. Given some input vector space  $V_{\text{in}}$  with representation  $\rho_{\text{in}}$  and some output space  $V_{\text{out}}$  with representation  $\rho_{\text{out}}$  the space of all equivariant linear layers mapping  $V_{\text{in}} \rightarrow V_{\text{out}}$  satisfies

$$\forall g \in G : \rho_{\text{out}}(g)W = W\rho_{\text{in}}(g).$$

These solutions to the constraint form a subspace of matrices  $\mathbb{R}^{n_{\text{out}} \times n_{\text{in}}}$  which can be solved for and described by a  $r$  dimensional orthonormal basis  $Q \in \mathbb{R}^{n_{\text{out}} n_{\text{in}} \times r}$ . Linear layers can then be parametrized in this equivariant basis. The elements of  $W$  can be parametrized  $\text{vec}(W) = Q\beta$  for  $\beta \in \mathbb{R}^r$  for the linear layer  $v \mapsto Wv$ , and symmetric biases can be parametrized similarly.

**Equivariance Priors with EMLP** In order to convert the hard equivariance constraints in EMLP into a soft prior over equivariance that can accommodate approximate symmetries, we can apply the RPP procedure from above to each these linear layers in the network. Instead of parametrizing the weights  $W$  directly in the equivariant basis  $\text{vec}(W) = Q\beta$ , we can instead define  $W$  as the sum  $W = A + B$  of an equivariant weight matrix  $\text{vec}(A) = Q\beta$  with a Gaussian prior over  $\beta$  and an unconstrained weight matrix  $B \sim \mathcal{N}(0, \sigma_b^2 I)$  with a Gaussian prior. A Gaussian prior over  $\beta \sim \mathcal{N}(0, \sigma_a^2 I)$  is equivalent to the Gaussian prior  $A \sim \mathcal{N}(0, \sigma_a^2 QQ^\top)$ . Since  $Q$  is an orthogonal matrix, we can breakdown the covariance of  $B$  into the covariance in the equivariant subspace  $Q$  as well as the covariance in the orthogonal complement  $P$ ,  $\sigma_b^2 I = \sigma_b^2 QQ^\top + \sigma_b^2 PP^\top$ . Therefore the sum of the weight matrices is distributed as  $A + B = W \sim \mathcal{N}(0, (\sigma_a^2 + \sigma_b^2)QQ^\top + \sigma_b^2 PP^\top)$ .

Regardless of the values of the prior variances  $\sigma_a^2$  and  $\sigma_b^2$ , solutions in the equivariant subspace  $QQ^\top$  are automatically favored by the model and assigned higher prior probability mass than those in the subspace  $PP^\top$  that violate the constraint. Even if  $\sigma_b > \sigma_a$ , the model still favors equivariance because the equivariance solutions are contained in the more flexible layer  $A$ . We show in Section 5.2 that RPPs are insensitive to the choice of  $\sigma_a$  and  $\sigma_b$ , provided that  $\sigma_a$  is large enough to be able to fit the data. By replacing each of the equivariant linear layers in an EMLP with a sum of an equivariant layer and an unconstrained layer and adding in the negative prior likelihood to the loss function, we produce an RPP-EMLP that can accommodate approximate or incorrectly specified symmetries.<sup>1</sup>

**RPPs With Other Equivariant Models** While in EMLP equivariant bases are solved for explicitly, the RPP can be applied to the linear layers in other equivariant networks in precisely the same way. A good example is the translationally equivariant convolutional neural network (CNN), which can be viewed as a restricted subset of a fully connected network. Though the layers are parametrized as convolutions, the convolution operation can be expressed as a Toeplitz matrix residing within the space of dense matrices. Adding the convolution to a fully connected layer and choosing a prior variance  $\sigma_a^2$  and  $\sigma_b^2$  over each, we have the same RPP prior

$$W \sim \mathcal{N}(0, \sigma_a^2 QQ^\top + \sigma_b^2 I) \tag{1}$$

where  $Q$  is the basis of (bi-)Toeplitz matrices corresponding to  $3 \times 3$  filters. This RPP CNN has the biases of convolution but can readily fit non translationally equivariant data. We can similarly create priors with the biases of other equivariant models like GCNNs [10], without any hard constraints. We can even apply the RPP principle to the breaking of a given symmetry group to a subgroup.

## 5 How and Why RPPs Work

We explore how and why RPPs work on a variety of domains, applying RPPs where (1) constraints are known to be helpful, (2) cannot fully describe the problem, and (3) are misspecified.

### 5.1 Dynamical Systems and Levels of Equivariance

In order to better understand how and why residual pathway priors interact with the symmetries of the problem we move to settings in which we can directly control both the type of symmetry and the

<sup>1</sup>For the EMLP that uses gated nonlinearities which do not always reduce to a standard Swish, we likewise add a more general Swish weighted by a parameter with prior variance  $\sigma_b^2$ .

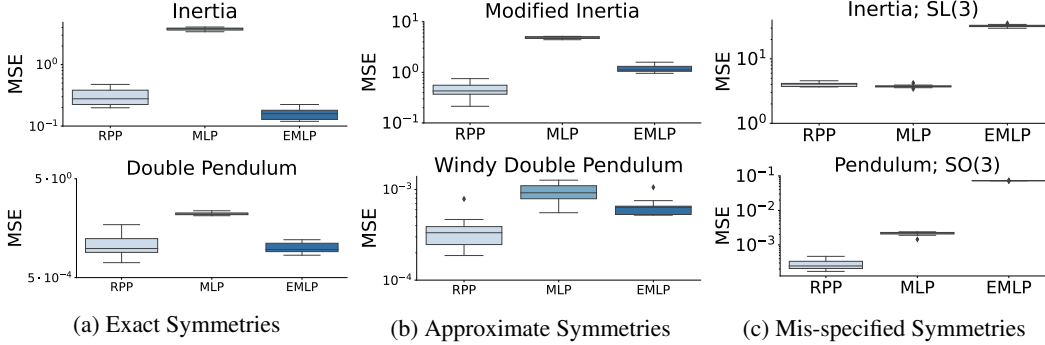


Figure 2: A comparison of test performance over 10 independent trials using RPP-EMLP and equivalent EMLP and MLP models on the inertia (**top**) and double pendulum (**bottom**) datasets in which we have three varying levels of symmetries. The boxes represent the interquartile range, and the whiskers the remainder of the distribution. **Left:** perfect symmetries in which EMLP and the equivariant components of RPP-EMLP exactly capture the symmetries in the data. **Center:** approximate symmetries in which the perfectly symmetric systems have been modified to include some non-equivariant components. **Right:** mis-specified symmetries in which the symmetric components of EMLP and RPP-EMLP do not reflect the symmetries present in the data.

level to which the symmetries are violated. We examine how RPPs coupled with EMLP networks (RPP-EMLP) perform on the inertia and double pendulum datasets featured in Finzi et al. [17] in 3 experimental settings: (i) the original inertia and double pendulum datasets which preserve exact symmetries with respect to the  $O(3)$  and  $O(2)$  groups respectively; (ii) modified versions of these datasets with additional factors (such as wind on the double pendulum) that lead to approximate symmetries; and (iii) versions with misspecified symmetry groups that break the symmetries entirely (described in Appendix C).

The results for these 3 settings are given in Figure 4. Across all settings RPP-EMLP match the performance of EMLP when symmetries are exact, perform as well as an MLP when the symmetry is misspecified and better than both when the symmetry is approximate. For these experiments we use a prior variance of  $\sigma_a^2 = 10^5$  on the EMLP weights and  $\sigma_b^2 = 1$  on the MLP weights.

**Exact Symmetries** As part of the motivation, RPPs should properly allocate prior mass to both constrained and unconstrained solutions, we test cases in which symmetries are exact, and show that RPP-EMLP is capable of performing on par with EMLP which only admits solutions with perfect symmetry. The results in Figure 4a show that although the prior over models as described RPP-EMLP is broader than that of EMLP (as we can admit non-equivariant solutions) in the presence of perfectly equivariant data RPP-EMLP do not hinder performance, and we are able to generalize nearly as well as the perfectly prescribed EMLP model.

**Approximate symmetries** To better showcase the ideas of Figure 1 we compare RPP-EMLPs to EMLPs and MLPs on the modified inertia and windy pendulum datasets. In these datasets we can think about the systems as primarily equivariant but containing non-equivariant contributions. As shown in 4b these problems are best suited for RPP-EMLP as MLPs have no bias towards the approximately symmetry present in the data, and EMLPs are overly constrained in this setting.

**Misspecified symmetries** In contrast to working with perfect symmetries and showing that RPP-EMLPs are competitive with EMLPs, we also show that when symmetries are *misspecified* the bias towards equivariant solutions does not hinder the performance of RPP-EMLPs. For the inertia dataset we substitute the group equivariance in EMLP from  $O(3)$  to the overly large group  $SL(3)$  consisting of all volume and orientation preserving linear transformations, not just the orthogonal ones. For the double pendulum dataset, we substitute  $O(2)$  symmetry acting on  $\mathbb{R}^3$  with the larger  $SO(3)$  rotation group that contains it but is not a symmetry of the dataset.

By purposefully misspecifying the symmetry in these datasets we intentionally construct EMLP and RPP-EMLP models with incorrect inductive biases. In this setting EMLP is incapable of making

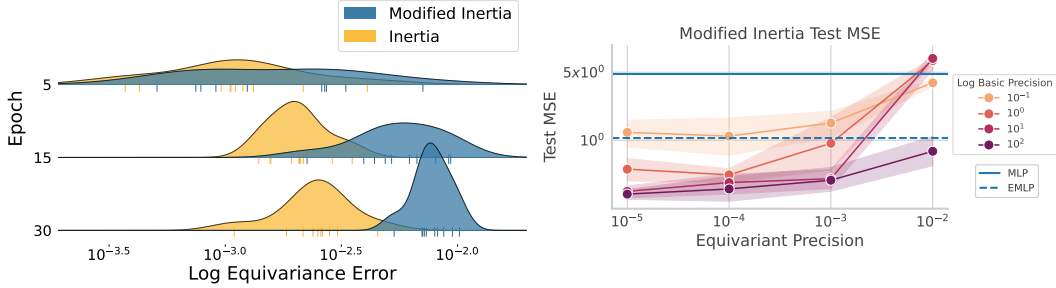


Figure 3: **Left:** Kernel density estimators of log equivariance error across training epochs for 10 independently trained networks. Here the color denotes the dataset these models were trained on. Treating these samples as a proxy for posterior density, we see that on the non-equivariant Modified Inertia dataset, the posterior is shifted upward to match the level of equivariance in the data during training. **Right:** Test MSE as a function of the weight decay parameters on the equivariant and basic weights on the modified inertia dataset. We observe that so long as the prior in the basis of equivariant weights is broad enough, we can achieve low test error with RPPs.

accurate predictions as it has a hard constraint on an incorrect symmetry. Figure 4c shows that even in cases where the model is intentionally mis-specified that RPPs can overcome a poorly aligned inductive bias and recover solutions that perform as well as standard MLPs, even where EMLPs fail.

## 5.2 Prior Levels of Equivariance

To test the effect of prior variances we use the modified inertia dataset, which represents a version of a problem in which perfect equivariance has been broken by adding new external forces to the dynamical system. Shown in Figure 3 (right) is a comparison of mean squared error on test data as a function of the prior precision terms on both the equivariance and basic weights. As a general trend we see that when the regularization on the equivariant weights is too high (equivalent to a concentrated prior around 0) we find instability in test performance, yet when we apply a broad prior to the equivariant weights performance is typically both better in terms of MSE, and more stable to the choice of prior on the basic model weights.

As the prior variances over the equivariant basis  $Q$  and the non-equivariant basis  $P$  describe our bias towards or away from equivariant solutions we investigate how the choice of prior variance relates to the level of symmetry present in a given dataset. In the windy pendulum dataset we have control over the level of wind and thus how far our system is from perfect equivariance.

## 5.3 Posterior Levels of Equivariance

RPPs describe a method for setting a prior over equivariance, and in the presence of new data we expect the posterior distribution over equivariance to change accordingly. Using samples from a deep ensemble to query points of high density in the posterior we estimate how the distribution over equivariance error progresses through training. Recalling that with an equivariant function  $f$  we have  $\rho_2(g)f(x) = f(\rho_1(g)x)$ , we compute equivariance error as

$$\text{EquivErr}(f, x) = \text{RelErr}(\rho_2(g)f(x), f(\rho_1(g)x)) \quad \text{where} \quad \text{RelErr}(a, b) = \frac{\|a - b\|}{\|a\| + \|b\|}. \quad (2)$$

We train one deep ensemble on the inertia dataset which exhibits perfect symmetry, and another on the modified inertia dataset which has only partial symmetry, with each deep ensemble being comprised of 10 individual models using the same procedure as in Section 5.1. In Figure 3 (left) we see that throughout training the models trained on the modified inertia concentrate around solutions with substantially higher equivariance error than models trained on the dataset with the exact symmetry. This figure demonstrates one of the core desiderata of RPPs: that we are able to converge to solutions with an appropriate level of equivariance for the data.

## 5.4 RPPs and Convolutional Structure

Using the RPP-Conv specified by the prior in Eqn 1 we apply the model to CIFAR-10 classification and UCI regression tasks where the inputs are reshaped to zero-padded two dimensional arrays and treated as images. Notably, the model is still an MLP and merely has larger prior variance in the convolutional subspace. As a result it can perform well on image datasets where the inductive bias is aligned, as well as on the UCI data despite not being an image dataset as shown in Table 1. While retaining the flexibility of an MLP, the RPP performs better than the locally connected MLPs trained with  $\beta$ -lasso in Neyshabur [42] which get 14% error on CIFAR-10. The full details for the architectures and training procedure are given in Appendix C.

	CIFAR-10	Energy	Fertility	Pendulum	Wine
MLP	$37.61 \pm 0.56$	$0.39 \pm 0.48$	$0.049 \pm 0.0044$	$4.65 \pm 0.50$	$0.66 \pm 0.058$
RPP	$12.62 \pm 0.34$	$0.73 \pm 0.44$	$0.060 \pm 0.0097$	$4.25 \pm 0.50$	$0.69 \pm 0.031$
Conv	$12.03 \pm 0.46$	$1.34 \pm 0.38$	$0.076 \pm 0.0157$	$4.63 \pm 0.36$	$0.79 \pm 0.092$

Table 1: Mean test classification error on CIFAR-10 and MSE on 4 UCI regression tasks, with one standard deviation errors taken over 10 trials. Similar to Figure 4, we find that whether the constrained convolutional structure is helpful (CIFAR) or not (UCI), RPP-Conv performs similarly to the model with the correct level of complexity.

## 6 Approximate Symmetries in Reinforcement Learning

Both model free and model based reinforcement learning present opportunities to take advantage of structure in the data for predictive power and data efficiency. On the one hand stands the use of model predictive control in the engineering community where finely specified dynamics models are constructed by engineers and only a small number of parameters are fit with system identification to determine mass, inertia, joint stiffness, etc. On the other side of things stands the hands off approach taken in the RL community, where general and unstructured neural networks are used for both transition models [9, 55, 25] as well as policies and value functions [20]. The state and action spaces for these systems are highly complex with many diverse inputs like quaternions, joint angles, forces, torques that each transform in different ways under a symmetry transformation like a left-right reflection or a rotation. As a result, most RL methods treat these spaces a black box ignoring all of this structure, and as a result they tend to require tremendous amounts of training data, making it difficult to apply to real systems without the use of simulators.

We can make use of this information about what kinds of objects populate the state and action spaces to encode approximate symmetries of the RL environments. As shown in van der Pol et al. [52], exploiting symmetries in MDPs by using equivariant networks can yield substantial improvements in data efficiency. But symmetries are brittle, and minor effects like rewards for moving in one direction, gravity, or even perturbations like wind, a minor tilt angle in CartPole, or other environment imperfections can break otherwise perfectly good symmetries. As shown in Table 2, broadening the scope to approximate symmetries allows for leveraging a lot more structure in the data which we can exploit with RPP. While Walker2d, Swimmer, Ant, and Humanoid have exact left/right reflection symmetries, Hopper, HalfCheetah, and Swimmer have approximate front/back reflection symmetries. Ant and Humanoid have an even more diverse set, with the  $D_4$  dihedral symmetry by reflecting and cyclicly permuting the legs of the ant, as well as continuous rotations of the Ant and Humanoid within the environment which can be broken by external forces or rewards. Identifying this structure in the data, we are able to use the generality of EMLP to construct an equivariant model for this data, and then turn it into a soft prior using RPP.

### 6.1 Approximate Symmetries in Model Free Reinforcement Learning

We evaluate RPPs on the standard suite of Mujoco continuous control tasks in the context of model-free reinforcement learning. With the appropriately specified action and state representations detailed in Appendix D, we construct RPP-EMLPs which we use as a drop-in replacement for both the policy and Q-function in the Soft Actor Critic (SAC) algorithm [20], using the same number of layers and



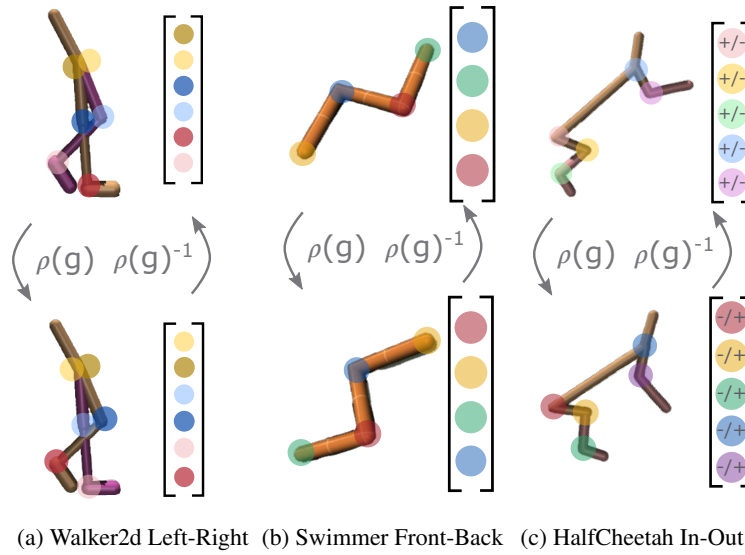


Figure 4: Example illustrations of symmetries and representations from the Mujoco environments. **Left:** left-right symmetry in the *Walker2d* environment, **center:** front-back symmetry in the *Swimmer* environment, and **right:** In-out similarity in the *HalfCheetah* environment

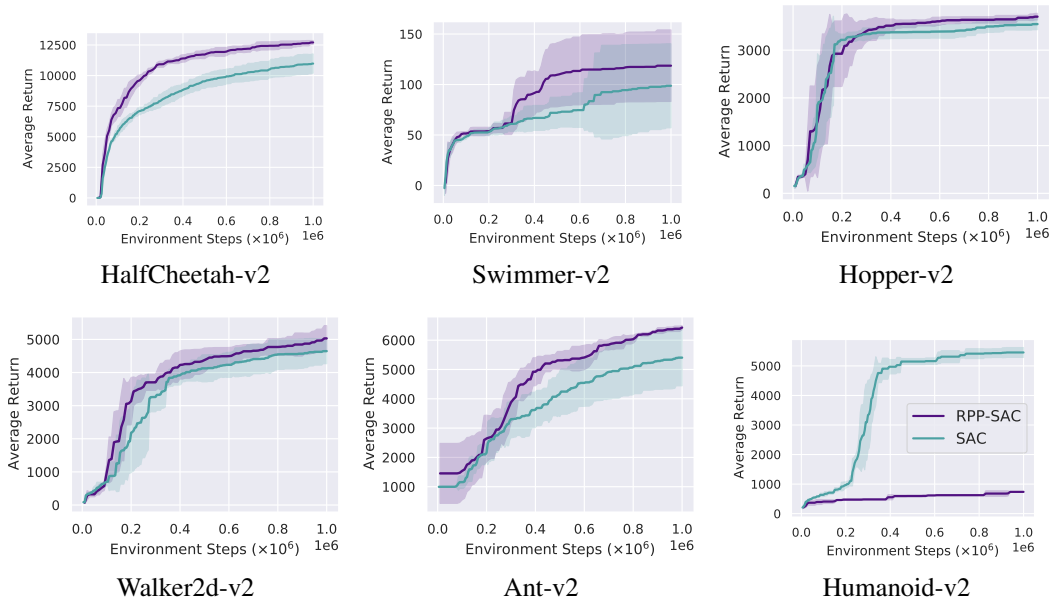


Figure 5: Average reward curve of RPP-SAC and SAC trained on Mujoco locomotion environments (max average reward attained at each step). Mean and one standard deviation taken over 4 trials shown in the shaded region. Incorporating approximate symmetries in the environments improves the efficiency of the model free RL agents.

Symmetries	Walker2d	Hopper	HalfCheetah	Swimmer	Ant	Humanoid
Exact	$\mathbb{Z}_2$	$\times$	$\times$	$\mathbb{Z}_2$	$\mathbb{Z}_2$	$\mathbb{Z}_2$
Approximate	$\mathbb{Z}_2$	$\mathbb{Z}_2$	$\mathbb{Z}_2$	$\mathbb{Z}_2 \times \mathbb{Z}_2$	$D_4 \times O(2)$	$\mathbb{Z}_2 \times O(2)$
This work	$\mathbb{Z}_2$	$\mathbb{Z}_2$	$\mathbb{Z}_2$	$\mathbb{Z}_2 \times \mathbb{Z}_2$	$\mathbb{Z}_4$	$SO(2)$

Table 2: Exact and approximate symmetries of Mujoco locomotion environments of which we use the subgroups in the bottom row, see Appendix D for the detailed action and state representations.

channels. In contrast with van der Pol et al. [52] where equivariance is used just for policies, we find that using RPP-EMLP for the policy function alone is not very helpful with Actor Critic (see Figure 5). With the exception of the Humanoid-v2 environment where the RPP-EMLP destabilizes SAC, we find that incorporating the exact and approximate equivariance with RPP yields consistent improvements in the data efficiency of the RL agent as shown in Figure 5.

## 6.2 Better Transition Models for Model Based Reinforcement Learning

	Swimmer-v2		Hopper-v2		Ant-v2	
Rollout	MLP	<b>RPP</b>	MLP	<b>RPP</b>	MLP	RPP
10 Steps	$0.51 \pm 0.02$	<b><math>0.40 \pm 0.04</math></b>	$1.1 \pm 0.1$	<b><math>0.9 \pm 0.1</math></b>	<b><math>4.2 \pm 0.1</math></b>	$5.2 \pm 0.3$
30 Steps	$1.6 \pm 0.2$	<b><math>1.26 \pm 0.14</math></b>	$3.8 \pm 0.3$	<b><math>3.1 \pm 0.5</math></b>	<b><math>11.3 \pm 0.2</math></b>	$13.9 \pm 0.7$
100 Steps	$3.9 \pm 1.0$	<b><math>2.75 \pm 0.31</math></b>	$9.8 \pm 0.5$	<b><math>7.0 \pm 0.7</math></b>	<b><math>16.0 \pm 0.3</math></b>	$20.0 \pm 1.1$
Equiv Err	46%	19%	98%	32%	36%	31%

Table 3: Transition model rollout relative error in percent % averaged over 10, 30, and 100 step rollouts (geometric mean over trajectory). Errorbars are 1 standard deviation taken over 3 random seeds. Equivariance error is computed from as the geometric mean averaged over the 100 step rollout.

We also investigate whether the equivariance prior of RPP can improve the quality of the predictions for transition models in the context of model based RL. To evaluate this in a way decoupled from the complex interactions between policy, model, and value function in MBRL, we instead construct a static dataset of 50,000 state transitions sampled uniformly from the replay buffer of a trained SAC agent. Since the trajectories in the replay buffer come from different times, they capture the varied dynamics MBRL transition models often encounter during training.

State of the art model based approaches on Mujoco tend to use an ensemble of small MLPs that predict the state transitions [9, 55, 25, 2], without exploiting any structure of the state space. We evaluate test rollout predictions via the relative error of the state over different length horizons for the RPP model against an MLP, the method of choice. As shown in Table 3, RPP transition models outperform MLPs on the Swimmer and Hopper environments, especially for long rollouts showing promise for use in MBRL. On these environments, RPP learns a smaller but non-negligible equivariance error that still enables it to fit the data.

## 7 Limitations

Using RPP-EMLP for the state and action spaces of the Mujoco environments required identifying the meaning of each of the components in terms of whether they are scalars, velocity vectors, joint angles, or orientation quaternions, and also which part of the robot they correspond to. This can be an error-prone process. While RPPs are fairly robust to such mistakes, the need to identify components makes using RPP more challenging than standard MLP. Additionally, due to the bilinear layers within EMLP, the Lipschitz constant of the network is unbounded which can lead to training instabilities when the inputs are not well normalized. We hypothesize these factors may contribute to the training instability we experienced using RPP-EMLP on Humanoid-v2.

## 8 Conclusion

In this work we have presented a method for converting restriction priors such as equivariance constraints into flexible models that have a bias towards structure but are not constrained by it. Given uncertainty about the nature of the data, RPPs are a safe choice. These RPP models are able to perform as well as the equivariant models when exact symmetries are present, and as well as unstructured MLPs when the specified symmetry is absent, and better than both for approximate symmetries. We have shown that encoding approximate symmetries can be a powerful technique for improving performance in a variety of settings, particularly for the messy and complex state and action spaces in reinforcement learning.

We hope that RPP enables designing more expressive priors for neural networks that capture the kinds of high level assumptions that machine learning researchers actually hold when developing models, rather than low level characteristics about the parameters that are hard to interpret. Building better techniques for enforcing high level properties helps lower the cost of incorporating prior knowledge, and better accommodate the complexities of data, even if they don't match our expectations.

**Acknowledgements** We thank Samuel Stanton for useful discussion and feedback. This research was supported by an Amazon Research Award, NSF I-DISRE 193471, NIH R01DA048764-01A1, NSF IIS-1910266, and NSF 1922658NRT-HDR: FUTURE Foundations, Translation, and Responsibility for Data Science.

## References

- [1] Farzad Abdohosseini, Hung Yu Ling, Zhaoming Xie, Xue Bin Peng, and Michiel van de Panne. On learning symmetric locomotion. In *Motion, Interaction and Games*, pages 1–10. 2019.
- [2] Brandon Amos, Samuel Stanton, Denis Yarats, and Andrew Gordon Wilson. On the model-based stochastic value gradient for continuous reinforcement learning. *arXiv preprint arXiv:2008.12775*, 2020.
- [3] Brandon Anderson, Truong Son Hy, and Risi Kondor. Cormorant: Covariant molecular neural networks. In *Advances in Neural Information Processing Systems*, pages 14510–14519, 2019.
- [4] Marcin Andrychowicz, Anton Raichuk, Piotr Stańczyk, Manu Orsini, Sertan Girgin, Raphael Marinier, Léonard Hussenot, Matthieu Geist, Olivier Pietquin, Marcin Michalski, et al. What matters in on-policy reinforcement learning? a large-scale empirical study. *arXiv preprint arXiv:2006.05990*, 2020.
- [5] Gregory Benton, Marc Finzi, Pavel Izmailov, and Andrew Gordon Wilson. Learning invariances in neural networks. *arXiv preprint arXiv:2010.11882*, 2020.
- [6] Alexander Bogatskiy, Brandon Anderson, Jan Offermann, Marwah Roussi, David Miller, and Risi Kondor. Lorentz group equivariant neural network for particle physics. In *International Conference on Machine Learning*, pages 992–1002. PMLR, 2020.
- [7] Greg Brockman, Vicki Cheung, Ludwig Pettersson, Jonas Schneider, John Schulman, Jie Tang, and Wojciech Zaremba. Openai gym. *arXiv preprint arXiv:1606.01540*, 2016.
- [8] Ricky TQ Chen, Yulia Rubanova, Jesse Bettencourt, and David K Duvenaud. Neural ordinary differential equations. In *Advances in neural information processing systems*, pages 6571–6583, 2018.
- [9] Kurtland Chua, Roberto Calandra, Rowan McAllister, and Sergey Levine. Deep reinforcement learning in a handful of trials using probabilistic dynamics models. *arXiv preprint arXiv:1805.12114*, 2018.
- [10] Taco Cohen and Max Welling. Group equivariant convolutional networks. In *International conference on machine learning*, pages 2990–2999. PMLR, 2016.
- [11] Zihang Dai, Hanxiao Liu, Quoc V Le, and Mingxing Tan. Coatnet: Marrying convolution and attention for all data sizes. *arXiv preprint arXiv:2106.04803*, 2021.

- [12] Stéphane d’Ascoli, Hugo Touvron, Matthew Leavitt, Ari Morcos, Giulio Biroli, and Levent Sagun. Convit: Improving vision transformers with soft convolutional inductive biases. *arXiv preprint arXiv:2103.10697*, 2021.
- [13] Alexey Dosovitskiy, Lucas Beyer, Alexander Kolesnikov, Dirk Weissenborn, Xiaohua Zhai, Thomas Unterthiner, Mostafa Dehghani, Matthias Minderer, Georg Heigold, Sylvain Gelly, et al. An image is worth 16x16 words: Transformers for image recognition at scale. *arXiv preprint arXiv:2010.11929*, 2020.
- [14] Dheeru Dua and Casey Graff. UCI machine learning repository, 2017. URL <http://archive.ics.uci.edu/ml>.
- [15] Bryn Elesedy and Sheheryar Zaidi. Provably strict generalisation benefit for equivariant models. *arXiv preprint arXiv:2102.10333*, 2021.
- [16] Marc Finzi, Samuel Stanton, Pavel Izmailov, and Andrew Gordon Wilson. Generalizing convolutional neural networks for equivariance to lie groups on arbitrary continuous data. In *International Conference on Machine Learning*, pages 3165–3176. PMLR, 2020.
- [17] Marc Finzi, Max Welling, and Andrew Gordon Wilson. A practical method for constructing equivariant multilayer perceptrons for arbitrary matrix groups. *arXiv preprint arXiv:2104.09459*, 2021.
- [18] Fabian B Fuchs, Daniel E Worrall, Volker Fischer, and Max Welling. Se (3)-transformers: 3d roto-translation equivariant attention networks. *arXiv preprint arXiv:2006.10503*, 2020.
- [19] Samuel Greydanus, Misko Dzamba, and Jason Yosinski. Hamiltonian neural networks. In *Advances in Neural Information Processing Systems*, pages 15379–15389, 2019.
- [20] Tuomas Haarnoja, Aurick Zhou, Pieter Abbeel, and Sergey Levine. Soft actor-critic: Off-policy maximum entropy deep reinforcement learning with a stochastic actor. In *International Conference on Machine Learning*, pages 1861–1870. PMLR, 2018.
- [21] Tuomas Haarnoja, Aurick Zhou, Pieter Abbeel, and Sergey Levine. Soft actor-critic: Off-policy maximum entropy deep reinforcement learning with a stochastic actor. In *International Conference on Machine Learning*, pages 1861–1870. PMLR, 2018.
- [22] Tuomas Haarnoja, Aurick Zhou, Kristian Hartikainen, George Tucker, Sehoon Ha, Jie Tan, Vikash Kumar, Henry Zhu, Abhishek Gupta, Pieter Abbeel, et al. Soft actor-critic algorithms and applications. *arXiv preprint arXiv:1812.05905*, 2018.
- [23] Kaiming He, Xiangyu Zhang, Shaoqing Ren, and Jian Sun. Deep residual learning for image recognition. In *Proceedings of the IEEE conference on computer vision and pattern recognition*, pages 770–778, 2016.
- [24] Kaiming He, Xiangyu Zhang, Shaoqing Ren, and Jian Sun. Identity mappings in deep residual networks. In *European conference on computer vision*, pages 630–645. Springer, 2016.
- [25] Michael Janner, Justin Fu, Marvin Zhang, and Sergey Levine. When to trust your model: Model-based policy optimization. *arXiv preprint arXiv:1906.08253*, 2019.
- [26] Jiechuan Jiang, Chen Dun, Tiejun Huang, and Zongqing Lu. Graph convolutional reinforcement learning. *arXiv preprint arXiv:1810.09202*, 2018.
- [27] Tobias Johannink, Shikhar Bahl, Ashvin Nair, Jianlan Luo, Avinash Kumar, Matthias Loskyll, Juan Aparicio Ojea, Eugen Solowjow, and Sergey Levine. Residual reinforcement learning for robot control. In *2019 International Conference on Robotics and Automation (ICRA)*, pages 6023–6029. IEEE, 2019.
- [28] K Kashinath, M Mustafa, A Albert, JL Wu, C Jiang, S Esmailzadeh, K Azizzadenesheli, R Wang, A Chattopadhyay, A Singh, et al. Physics-informed machine learning: case studies for weather and climate modelling. *Philosophical Transactions of the Royal Society A*, 379(2194): 20200093, 2021.

- [29] Diederik P Kingma and Jimmy Ba. Adam: A method for stochastic optimization. *arXiv preprint arXiv:1412.6980*, 2014.
- [30] Ilya Kostrikov, Denis Yarats, and Rob Fergus. Image augmentation is all you need: Regularizing deep reinforcement learning from pixels. *arXiv preprint arXiv:2004.13649*, 2020.
- [31] Alex Krizhevsky, Geoffrey Hinton, et al. Learning multiple layers of features from tiny images. 2009.
- [32] Yann LeCun, Bernhard Boser, John S Denker, Donnie Henderson, Richard E Howard, Wayne Hubbard, and Lawrence D Jackel. Backpropagation applied to handwritten zip code recognition. *Neural computation*, 1(4):541–551, 1989.
- [33] Yijiong Lin, Jiancong Huang, Matthieu Zimmer, Yisheng Guan, Juan Rojas, and Paul Weng. Invariant transform experience replay: Data augmentation for deep reinforcement learning. *IEEE Robotics and Automation Letters*, 5(4):6615–6622, 2020.
- [34] Iou-Jen Liu, Raymond A Yeh, and Alexander G Schwing. Pic: permutation invariant critic for multi-agent deep reinforcement learning. In *Conference on Robot Learning*, pages 590–602. PMLR, 2020.
- [35] Rosanne Liu, Joel Lehman, Piero Molino, Felipe Petroski Such, Eric Frank, Alex Sergeev, and Jason Yosinski. An intriguing failing of convolutional neural networks and the coordconv solution. *arXiv preprint arXiv:1807.03247*, 2018.
- [36] Ziming Liu, Yunyue Chen, Yuanqi Du, and Max Tegmark. Physics-augmented learning: A new paradigm beyond physics-informed learning. *arXiv preprint arXiv:2109.13901*, 2021.
- [37] David JC MacKay and David JC Mac Kay. *Information theory, inference and learning algorithms*. Cambridge university press, 2003.
- [38] Haggai Maron, Heli Ben-Hamu, Nadav Shamir, and Yaron Lipman. Invariant and equivariant graph networks. *arXiv preprint arXiv:1812.09902*, 2018.
- [39] Haggai Maron, Or Litany, Gal Chechik, and Ethan Fetaya. On learning sets of symmetric elements. *arXiv preprint arXiv:2002.08599*, 2020.
- [40] Aditi Mavalankar. Goal-conditioned batch reinforcement learning for rotation invariant locomotion. *arXiv preprint arXiv:2004.08356*, 2020.
- [41] Takeru Miyato, Toshiki Kataoka, Masanori Koyama, and Yuichi Yoshida. Spectral normalization for generative adversarial networks. *arXiv preprint arXiv:1802.05957*, 2018.
- [42] Behnam Neyshabur. Towards learning convolutions from scratch. *arXiv preprint arXiv:2007.13657*, 2020.
- [43] Behnam Neyshabur, Ryota Tomioka, and Nathan Srebro. In search of the real inductive bias: On the role of implicit regularization in deep learning. *arXiv preprint arXiv:1412.6614*, 2014.
- [44] Prajit Ramachandran, Barret Zoph, and Quoc V Le. Searching for activation functions. *arXiv preprint arXiv:1710.05941*, 2017.
- [45] Balaraman Ravindran and Andrew G Barto. Approximate homomorphisms: A framework for non-exact minimization in markov decision processes. 2004.
- [46] David E Rumelhart, Geoffrey E Hinton, and Ronald J Williams. Learning internal representations by error propagation. Technical report, California Univ San Diego La Jolla Inst for Cognitive Science, 1985.
- [47] Victor Garcia Satorras, Emiel Hoogeboom, and Max Welling. E (n) equivariant graph neural networks. *arXiv preprint arXiv:2102.09844*, 2021.
- [48] Tom Silver, Kelsey Allen, Josh Tenenbaum, and Leslie Kaelbling. Residual policy learning. *arXiv preprint arXiv:1812.06298*, 2018.

- [49] Sainbayar Sukhbaatar, Arthur Szlam, and Rob Fergus. Learning multiagent communication with backpropagation. *arXiv preprint arXiv:1605.07736*, 2016.
- [50] Jonathan Taylor, Doina Precup, and Prakash Panagaden. Bounding performance loss in approximate mdp homomorphisms. *Advances in Neural Information Processing Systems*, 21: 1649–1656, 2008.
- [51] Elise van der Pol, Thomas Kipf, Frans A Oliehoek, and Max Welling. Plannable approximations to mdp homomorphisms: Equivariance under actions. *arXiv preprint arXiv:2002.11963*, 2020.
- [52] Elise van der Pol, Daniel Worrall, Herke van Hoof, Frans Oliehoek, and Max Welling. Mdp homomorphic networks: Group symmetries in reinforcement learning. *Advances in Neural Information Processing Systems*, 33, 2020.
- [53] Mark van der Wilk, Matthias Bauer, ST John, and James Hensman. Learning invariances using the marginal likelihood. *arXiv preprint arXiv:1808.05563*, 2018.
- [54] Renhao Wang, Marjan Albooyeh, and Siamak Ravanbakhsh. Equivariant maps for hierarchical structures. *arXiv preprint arXiv:2006.03627*, 2020.
- [55] Tingwu Wang and Jimmy Ba. Exploring model-based planning with policy networks. *arXiv preprint arXiv:1906.08649*, 2019.
- [56] Maurice Weiler and Gabriele Cesa. General  $e(2)$ -equivariant steerable cnns. *arXiv preprint arXiv:1911.08251*, 2019.
- [57] Andrew Gordon Wilson and Pavel Izmailov. Bayesian deep learning and a probabilistic perspective of generalization. In *Advances in Neural Information Processing Systems*, 2020.
- [58] Daniel E Worrall, Stephan J Garbin, Daniyar Turmukhambetov, and Gabriel J Brostow. Harmonic networks: Deep translation and rotation equivariance. In *Proceedings of the IEEE Conference on Computer Vision and Pattern Recognition*, pages 5028–5037, 2017.
- [59] Tete Xiao, Piotr Dollar, Mannat Singh, Eric Mintun, Trevor Darrell, and Ross Girshick. Early convolutions help transformers see better. In *Thirty-Fifth Conference on Neural Information Processing Systems*, 2021.
- [60] Manzil Zaheer, Satwik Kottur, Siamak Ravanbakhsh, Barnabas Poczos, Russ R Salakhutdinov, and Alexander J Smola. Deep sets. In *Advances in neural information processing systems*, pages 3391–3401, 2017.
- [61] Yanzhao Zhou, Qixiang Ye, Qiang Qiu, and Jianbin Jiao. Oriented response networks. In *Proceedings of the IEEE Conference on Computer Vision and Pattern Recognition*, pages 519–528, 2017.

# Residual Pathway Priors for Soft Equivariance Constraints

## Supplementary Material

### Appendix Outline

In Section 7 discuss potential for negative impact. In Section B we investigate the utility of using RPP-EMLP for the policy function only on the Mujoco tasks. In Section C we detail the datasets and experimental methodology used in the paper. Finally in Sections D and E we break down the components of the Mujoco environment state and action spaces, and the representations that we use for them.

### A Potential Negative Impacts

As one of our primary application areas is reinforcement learning, and specifically exploiting approximate symmetries in reinforcement learning, we must address the potential negative impacts of the deployment of RPPs in RL systems. In general model free RL algorithms tend to be brittle, and often policies and behavior learned in a simulated environment like Mujoco don't transfer easily to real world robots. This point is acknowledged by most RL researchers, and a large effort is being made to improve the situation. Applying neural networks to the control of real robots can be dangerous if the functions are important or failure can cause injury to the robot or humans. We believe that RL will ultimately be impactful for robot control, however practitioners need to be responsible and exercise caution.

### B Benefit of Equivariant Value Functions

In principle both the policy and the value or critic function can benefit from equivariance. However, the policy learns from the value function in the policy update which is approximately equivalent to minimizing the KL divergence

$$\mathbb{E}_{s \sim \mathcal{D}}[\text{KL}(\pi_\phi(\cdot|s) | \exp(Q_\theta(\cdot, s))/Z_\theta(s))]$$

as derived in Haarnoja et al. [21]. If the value function  $Q$  is a standard MLP yielding a non equivariant distribution and the policy function  $\pi$  is an RPP that merely has a bias towards equivariance, then the RPP policy will learn to fit the non equivariant parts of  $Q$  as if it were a ground truth dataset that is not equivariant. This likely explains why we find in practice that using an RPP for the value function has a stronger impact on performance as shown in Figure 5.

### C Experimental Details

Here we present the training details of the models used in the paper. Experiments were run on private servers with NVIDIA Titan RTX and RTX 2080 Ti GPUs. We estimate that all runs performed in the initial experimentation and final evaluation on the RL tasks used approximately 500 GPU hours. The experiments on dynamical systems, CIFAR-10, and UCI data required an additional 200 GPU hours.

#### C.1 Synthetic Dataset Experiments (5.1 and 5.3)

The windy pendulum dataset is a variant of the double spring pendulum Hamiltonian system from Finzi et al. [17]. In addition to the Hamiltonian of the base system

$$H_0(x_1, x_2, p_1, p_2) = V(x_1, x_2) + T(p_1, p_2)$$

where  $T(p_1, p_2) = \|p_1\|^2/2m_1 + \|p_2\|^2/2m_2$  and  $V(x_1, x_2) =$

$$\frac{1}{2}k_1(\|x_1\| - \ell_1)^2 + \frac{1}{2}k_2(\|x_1 - x_2\| - \ell_2)^2 + m_1g^\top x_1 + m_2g^\top x_2,$$

we add a perturbation  $H_1(x_1, x_2, p_1, p_2) = -w^\top x_1 - w^\top x_2$  that is the energy of the wind acting as a constant force pushing in the  $w = [-8, -5, 0]$  direction. Setting  $H = H_0 + \epsilon H_1$ , we can control the strength of the wind and we choose  $\epsilon = 0.01$ . This perturbation breaks the  $\text{SO}(2)$  symmetry about the  $z$  axis.

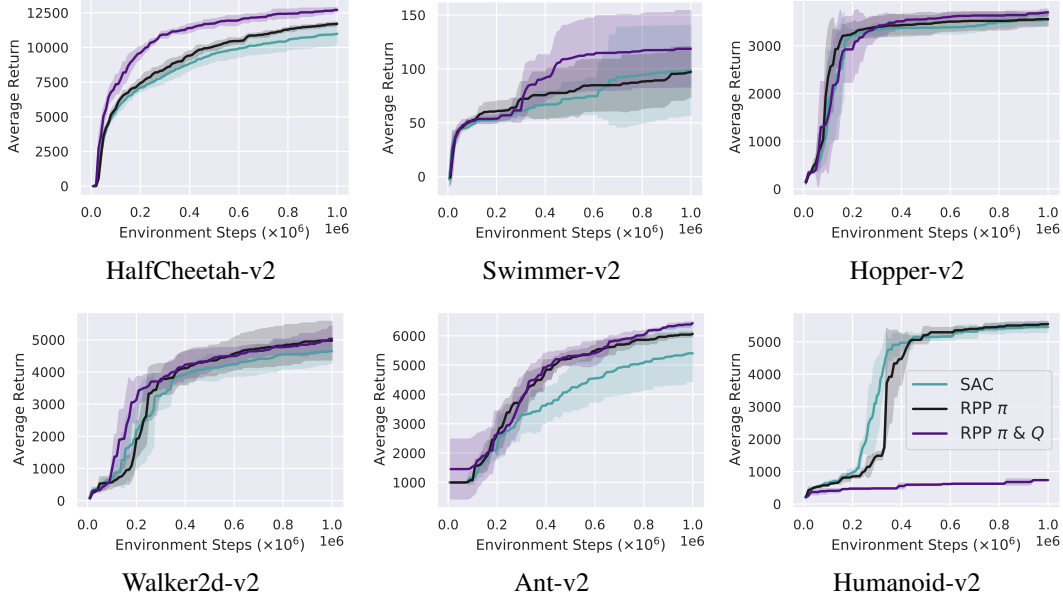


Figure 6: Average reward curves (max over steps) for an RPP-EMLP applied to the policy  $\pi$  only, as well as an RPP-EMLP for both the policy  $\pi$  and the critic  $Q$ . Mean and standard deviation taken over 4 trials shown in the shaded region. Only minor performance gains are achieved if using RPP for the policy only, however this variant is more stable and can to train on Humanoid-v2 without diverging.

For the MLP, EMLP, and RPP we use 3 layer deep 128 hidden unit Hamiltonian neural networks [19] to fit the data using the rollouts of an ODE integrator [8] with an MSE loss on rollouts of length 5 timesteps with  $\Delta t = 0.2$ . For training we use 500 trajectory chunks and use another 500 for testing. We train all models in section 5.1 for 1000 epochs, sufficient for convergence. The input and output representation for EMLP and RPP-EMLP is  $V_{O(3)}^4 \rightarrow \mathbb{R}$ , where  $V_{O(3)}$  is the restricted representation from the standard representation of a 3D rotation matrix to the given group in question, like  $SO(2)$  for rotations about the  $z$  axis. The input is  $V_{O(3)}^4$  because there are two point masses each of which has a 3D vectors for position and for momentum. The scalar  $\mathbb{R}$  output is the Hamiltonian function.

The Modified Inertia dataset is a small regression dataset off of the task also from Finzi et al. [17] for learning the moment of inertia matrix in 3D of a collection of 5 point masses. For the base Inertia dataset, the targets are  $\mathcal{I} = \sum_{i=1}^5 m_i(x_i^\top x_i I - x_i x_i^\top)$  from the input tuples  $(m_i, x_i)_{i=1}^5$ . In order to break the equivariance of the dataset, we add an additional term so that the target is  $y = \text{vec}(\mathcal{I} + 0.3\hat{z}\hat{z}^\top\mathcal{I})$  where  $\hat{z}$  is the unit vector along the  $z$  axis. The input and output representations for EMLP and RPP-EMLP on this problem are  $(\mathbb{R} \oplus V)^5 \rightarrow V \otimes V$ , representing the 5 point masses and vectors mapping to matrices  $V \otimes V$ .

We use 1000 train and test examples for the inertia datasets and we train for 500 epochs. In both cases we use an Adam optimizer [29] with a learning rate of 0.003.

## C.2 Image and UCI experiments (5.4)

We use the CIFAR-10 and UCI datasets, taken from Krizhevsky et al. [31] and Dua and Graff [14] respectively. In Section 5 we train models on dynamical systems and CIFAR-10 and UCI regression data. For the CIFAR-10 experiments we use a convolutional neural network (and the equivalent MLP) with 9 convolutional layers and 1 fully connected layer, and max-pooling layers after the third and sixth convolutional layers. The channel sizes of the 9 layers are, in order: 16, 16, 16, 32, 32, 32, 32, 32, 32. We train for 200 epochs using a cosine learning rate schedule with an initial learning rate of 0.05 and the Adam optimizer.

For the UCI tasks we use a small convolutional neural network, and the equivalent MLP, with 3 convolutional layers and 1 fully connected layer, with each convolutional layer having 32 channels.



Models are trained for 1000 epochs using an Adam optimizer with a learning rate of 0.01 and a cosine learning rate schedule.

### C.3 Model Free RL

We train on the Mujoco locomotion tasks in the OpenAI gym environments [7]. We follow the implementation details and hyperparameters from Haarnoja et al. [22], with a learned temperature function, stochastic policies, and double critics. Additionally we use the recommendation from Andrychowicz et al. [4] to initialize the last layer of the policy network with 100x smaller weights, which we find slightly improves the performance of both RPP and the baseline. Additionally for RPP which can be less stable than standard SAC, we use the Adam betas  $\beta_1 = 0.5$  and  $\beta_2 = 0.999$  that are used in the GAN community [41] rather than the defaults. Training with the RPP  $\pi$  and  $Q$  functions on the Mujoco locomotion tasks takes about 8 hours for 1 million steps.

We found it necessary to reduce the speed  $\tau$  of the critic moving average to keep SAC stable on some of the environments, with values shown in Table 4. In general, higher  $\tau$ 's are favorable for learning quickly. Unfortunately we were not able to get SAC with an RPP Q function to train reliably on Humanoid, even after trying multiple values of  $\tau$ .

	Walker2d	Hopper	HalfCheetah	Swimmer	Ant	Humanoid
Baseline $\tau$	.005	.005	.005	.005	.005	.005
RPP $\tau$	.004	.005	.005	.004	.005	$\times$

Table 4: Critic moving average speed  $\tau$ .

### C.4 Transition Models for Mujoco

We train the transition models on a dataset of 50000 transitions which are composed of 5000 trajectory chunks of length 10. These trajectory chunks are sampled uniformly from the replay buffer collected over the course of training a standard SAC agent for  $10^6$  steps on each of the environments. We train by minimizing the  $\ell_1$  norm of the rollout error over a 10 step trajectory, and we evaluate on a holdout set of 50 trajectories of length 100.

The models are simple MLPs or RPPs mapping from the state and control actions to the state space, predicting the change in state,

$$x_{t+1} = x_t + \text{NN}(x_t, u_t).$$

For the MLPs and RPPs we use 2 hidden layers of size 256 as well as swish activations [44]. We use a prior variance of  $10^6$  in the equivariant subspace and 3 in the non equivariant subspace. The RPP is a standard RPP-EMLP with the input representation  $\rho_X \oplus \rho_U$  (concatenation of the representation of the state space and the action space), output representation  $\rho_X$ , and symmetry group described in Appendix D the same as for the model free experiments. We train the transition models for 500 epochs which takes about 45 minutes for RPP compared to 15 minutes for the standard MLPs.

## D Mujoco State and Action Representations

Based on the state and action spaces of the Mujoco environments we describe in Appendix E, we define appropriate group representations on these spaces. Let  $V$  be the base representation of the group acted upon by permutations for  $\mathbb{Z}_n$  and by rotation matrices for  $\text{SO}(2)$ , let  $\mathbb{R}$  denote a scalar representation (of dimension 1) that is unaffected by the transformations, and let  $P$  be a pseudoscalar representation (of dimension 1) that transforms by the sign of the permutation. For  $\mathbb{Z}_2$ ,  $P$  takes the values 1 and  $-1$  and acts by negating the values when a flip or L/R reflection is applied.

From the raw state and action spaces listed in Appendix E, we convert quaternions to 3D rotation matrices for Humanoid and Ant, and we reorder elements to group together left/right pairs for Walker2d and Swimmer. The representations of these transformed state and action vectors are shown in Table 5. Note that  $V^3$  denotes  $V \oplus V \oplus V = V^{\oplus 3}$ , and is simply the concatenation of 3 copies of  $V$  as  $\mathbb{R}^3$  would be 3 copies of  $\mathbb{R}$ . This is not to be confused with powers of the tensor product,  $V^{\otimes 3} = V \otimes V \otimes V$ . For Humanoid, we denote the restricted representation of 3D rotation matrices restricted to the  $\text{SO}(2)$  rotations about the  $z$  axis as  $V_{\text{SO}(3)}$ .

Table 5: Mujoco Locomotion State and Action Representations used for RPP-EMLP

Env	State Representation	Action Rep	Group
Hopper	$\mathbb{R} \oplus P^5 \oplus \mathbb{R} \oplus P^4$	$P^3$	$\mathbb{Z}_2$
Swimmer	$\mathbb{R} \oplus P_{\leftrightarrow} \oplus (P_{\leftrightarrow} \otimes V_{\downarrow}) \oplus (\mathbb{R} \oplus P)^2 \oplus (P_{\leftrightarrow} \otimes V_{\downarrow})$	$P_{\leftrightarrow} \otimes V_{\downarrow}$	$\mathbb{Z}_2^{\leftrightarrow} \times \mathbb{Z}_2^{\downarrow}$
HalfCheetah	$\mathbb{R} \oplus P^8 \oplus \mathbb{R} \oplus P^7$	$P^6$	$\mathbb{Z}_2$
Walker2d	$\mathbb{R}^2 \oplus V^3 \oplus \mathbb{R}^3 \oplus V^3$	$V^3$	$\mathbb{Z}_2$
Ant	$\mathbb{R}^5 \oplus V^2 \oplus \mathbb{R}^6 \oplus V^2$	$V^2$	$\mathbb{Z}_4$
Humanoid	$\mathbb{R} \oplus V_{SO(3)}^{\otimes 2} \oplus \mathbb{R}^{17} \oplus V_{SO(3)}^2 \oplus \mathbb{R}^{17}$	$\mathbb{R}^{17}$	$SO(2)$

## E Mujoco State and Action Spaces

In order to build symmetries into the state and action representations for Mujoco environments, we need to have a detailed understanding of what the state and action spaces for these environments represent. As these spaces are not well documented, for each of the Mujoco environments we experimented in the simulator and identified the meanings of the state vectors in Tables 10, 12, 11, 7, 9, 6, and 8. We hope that these detailed descriptions can be useful to other researchers.

Table 6: Hopper-v2 State and Action Spaces

State Space	X (Unobserved)
	Y
	Orientation Angle
	Hip Angle
	Knee Angle
	Ankle Angle
	X Velocity
	Y Velocity
	Orientation Angular Velocity
	Hip Angular Velocity
	Knee Angular Velocity
	Ankle Angular Velocity
Action Space	Hip
	Knee
	Ankle

Table 7: Swimmer-v2 State and Action Spaces

State Space	X (Unobserved)	
	Y (Unobserved)	
	Orientation Angle	
	Head Joint Angle	
	Tail Joint Angle	
	X Velocity	
	Y Velocity	
	Orientation Angular Velocity	
	Head Joint Angular Velocity	
	Tail Joint Angular Velocity	
	Action Space	Head Joint
		Tail Joint

Table 8: HalfCheetah-v2 State and Action Spaces

State Space	X (Unobserved)
	Y
	Orientation Angle
	Rear Hip Angle
	Rear Knee Angle
	Rear Ankle Angle
	Front Hip Angle
	Front Knee Angle
	Front Ankle Angle
	X Velocity
	Y Velocity
	Orientation Angular Velocity
	Rear Hip Angular Velocity
	Rear Knee Angular Velocity
	Rear Ankle Angular Velocity
	Front Hip Angular Velocity
Front Knee Angular Velocity	
Front Ankle Angular Velocity	
Action Space	Rear Hip
	Rear Knee
	Rear Ankle
	Front Hip
	Front Knee
	Front Ankle

Table 9: Walker2d-v2 State and Action Spaces

State Space	X (Unobserved)
	Y
	Orientation Angle
	Right Hip Angle
	Right Knee Angle
	Right Ankle Angle
	Left Hip Angle
	Left Knee Angle
	Left Ankle Angle
	X Velocity
	Y Velocity
	Orientation Angular Velocity
	Right Hip Angular Velocity
	Right Knee Angular Velocity
	Right Ankle Angular Velocity
	Left Hip Angular Velocity
Left Knee Angular Velocity	
Left Ankle Angular Velocity	
Action Space	Right Hip
	Right Knee
	Right Ankle
	Left Hip
	Left Knee
	Left Ankle

Table 10: Ant-v2 State and Action Spaces

State Space	X (Unobserved)
	Y (Unobserved)
	Z
	Orientation Quaternion ( $4D$ )
	Limb 2 Left/Right
	Limb 2 Up/Down
	Limb 3 Left/Right
	Limb 3 Up/Down
	Limb 4 Left/Right
	Limb 4 Up/Down
Action Space	Limb 1 Left/Right
	Limb 1 Up/Down
	Limb 1 Left/Right
	Limb 1 Up/Down
	Limb 2 Left/Right
	Limb 2 Up/Down
	Limb 3 Left/Right
	Limb 3 Up/Down
Limb 4 Left/Right	
Limb 4 Up/Down	

Table 11: Humanoid-v2 Action Space

Action Space	Torso Forward/Backward
	Torso Z
	Torso Left/Right
	Right Hip Left/Right
	Right Hip Up/Down
	Right Hip Front/Back
	Right Knee Front/Back
	Left Hip Left/Right
	Left Hip Up/Down
	Left Hip Front/Back
	Left Knee Front/Back
	Right Shoulder Left/Right
	Right Shoulder Front/Back
	Right Elbow Front/Back
	Left Shoulder Left/Right
	Left Shoulder Front/Back
	Left Elbow Front/Back

Table 12: Humanoid-v2 State Space

State Space (Position)	X (Unobserved)	
	Y (Unobserved)	
	Z	
	Orientation Quaternion ( $4D$ )	
	Torso Z	
	Torso Forward/Backward	
	Torso Left/Right	
	Right Hip Left/Right	
	Right Knee Left/Right	
	Right Hip Up/Down	
	Right Knee Up/Down	
	Left Hip Left/Right	
	Left Knee Left/Right	
	Left Hip Up/Down	
	Left Knee Up/Down	
	Right Shoulder Left/Right	
	Right Shoulder Up/Down	
	Right Elbow Left/Right	
	Left Shoulder Left/Right	
	Left Shoulder Up/Down	
	Left Elbow Left/Right	
	State Space (Velocity)	Body Linear Velocity ( $3D$ )
		Body Angular Velocity ( $3D$ )
		Torso Z
		Torso Forward/Backward
		Torso Left/Right
Right Hip Left/Right		
Right Knee Left/Right		
Right Hip Up/Down		
Right Knee Up/Down		
Left Hip Left/Right		
Left Knee Left/Right		
Left Hip Up/Down		
Left Knee Up/Down		
Right Shoulder Left/Right		
Right Shoulder Up/Down		
Right Elbow Left/Right		
Left Shoulder Left/Right		
Left Shoulder Up/Down		
Left Elbow Left/Right		